

Pressure-induced anomalous insulating behavior in frustrated iridate $La_3Ir_3O_{11}$

Chun-Hua Chen(陈春华), Yong-Hui Zhou(周永惠), Ying Zhou(周颖), Yi-Fang Yuan(袁亦方), Chao An(安超), Xu-Liang Chen(陈绪亮), Zhao-Ming Tian(田召明), and Zhao-Rong Yang(杨昭荣)

Citation: Chin. Phys. B, 2021, 30 (**6**): 067402. DOI: 10.1088/1674-1056/abf100

Journal homepage: http://cpb.iphy.ac.cn; http://iopscience.iop.org/cpb

What follows is a list of articles you may be interested in

Superconducting anisotropy and vortex pinning in $CaKFe_4As_4$ and $KCa_2Fe_4As_4F_2$

A B Yu(于奥博), Z Huang(黄喆), C Zhang(张驰), Y F Wu(吴宇峰), T Wang(王腾), T Xie(谢涛), C Liu(刘畅), H Li(李浩), W Peng(彭炜), H Q Luo(罗会仟), G Mu(牟刚), H Xiao(肖宏), L X You(尤立星), and T Hu(胡涛)

Chin. Phys. B, 2021, 30 (**2**): 027401. DOI: 10.1088/1674-1056/abcf98

Anisotropy of $Ca_{0.73}La_{0.27}(Fe_{0.96}Co_{0.04})As_2$ studied by torque magnetometry

Ya-Lei Huang(黄亚磊), Run Yang(杨润), Pei-Gang Li(李培刚), Hong Xiao(肖宏)

Chin. Phys. B, 2020, 29 (**9**): 097405. DOI: 10.1088/1674-1056/ab9f26

Advanced high-pressure transport measurement system integrated with low temperature and magnetic field

Jing Guo(郭静), Qi Wu(吴奇), Liling Sun(孙力玲)

Chin. Phys. B, 2018, 27 (**7**): 077402. DOI: 10.1088/1674-1056/27/7/077402

The structure and elasticity of phase B silicates under high pressure by first principles simulation

Lei Liu(刘雷), Li Yi(易丽), Hong Liu(刘红), Ying Li(李营), Chun-Qiang Zhuang(庄春强), Long-Xing Yang(杨龙星), Gui-Ping Liu(刘桂平)

Chin. Phys. B, 2018, 27 (**4**): 047402. DOI: 10.1088/1674-1056/27/4/047402

Structural, elastic, and vibrational properties of phase H: A first-principles simulation

Chao-Jia Lv(吕超甲), Lei Liu(刘雷), Yang Gao(高阳), Hong Liu(刘红), Li Yi(易丽), Chun-Qiang Zhuang(庄春强), Ying Li(李营),

Chin. Phys. B, 2017, 26 (**6**): 067401. DOI: 10.1088/1674-1056/26/6/067401

Pressure-induced anomalous insulating behavior in frustrated iridate $La_3Ir_3O_{11}$*

Chun-Hua Chen(陈春华)[1,2], Yong-Hui Zhou(周永惠)[1,†], Ying Zhou(周颖)[3], Yi-Fang Yuan(袁亦方)[1,2], Chao An(安超)[3], Xu-Liang Chen(陈绪亮)[1], Zhao-Ming Tian(田召明)[4], and Zhao-Rong Yang(杨昭荣)[1,3,5,‡]

[1] *Anhui Province Key Laboratory of Condensed Matter Physics at Extreme Conditions, High Magnetic Field Laboratory, Chinese Academy of Sciences, Hefei* 230031, *China*

[2] *Science Island Branch of Graduate School, University of Science and Technology of China, Hefei* 230026, *China*

[3] *Institutes of Physical Science and Information Technology, Anhui University, Hefei* 230601, *China*

[4] *School of Physics, and Wuhan National High Magnetic Field Center, Huazhong University of Science and Technology, Wuhan* 430074, *China*

[5] *High Magnetic Field Laboratory of Anhui Province, Hefei* 230031, *China*

(Received 21 February 2021; revised manuscript received 5 March 2021; accepted manuscript online 23 March 2021)

The geometrically frustrated iridate $La_3Ir_3O_{11}$ with strong spin–orbit coupling and fractional valence was recently predicted to be a quantum spin liquid candidate at ambient conditions. Here, we systematically investigate the evolution of structural and electronic properties of $La_3Ir_3O_{11}$ under high pressure. Electrical transport measurements reveal an abnormal insulating behavior rather than metallization above a critical pressure $P_c \sim 38.7$ GPa. Synchrotron x-ray diffraction (XRD) experiments indicate the stability of the pristine cubic $KSbO_3$-type structure up to 73.1 GPa. Nevertheless, when the pressure gradually increases across P_c, the bulk modulus gets enhanced and the pressure dependence of bond length d_{Ir-Ir} undergoes a slope change. Consistent with the XRD data, detailed analyses of Raman spectra reveal an abnormal redshift of Raman mode and a change of Raman intensity around P_c. Our results demonstrate that the pressure-induced insulating behavior in $La_3Ir_3O_{11}$ can be assigned to the structural modification, such as the distortion of IrO_6 octahedra. These findings will shed light on the emergent abnormal insulating behavior in other 5d iridates reported recently.

Keywords: high pressure, 5d iridates, semimetal–insulator transition, crystal structure

PACS: 74.62.Fj, 72.80.Ga, 71.30.+h, 74.62.Bf **DOI:** 10.1088/1674-1056/abf100

1. Introduction

The 5d transition metal oxides have recently attracted extensive interest due to their rich physical properties, including topological Mott insulator, topological Weyl semimetal, spin–orbital Mott insulator, quantum spin liquids (QSL), etc.[1–8] In iridate oxides, these emergent physical phenomena are not only triggered by a rare interplay of on-site Coulomb repulsion and strong spin–orbit coupling (SOC), but also strongly depending on specific crystal structures, e.g., Ruddlesden–Popper perovskite,[9] honeycomb,[6] pyrochlore,[10] and $KSbO_3$-type structure.[11] For instance, Ruddlesden–Popper Sr_2IrO_4 with Ir^{4+} ($5d^5$) exhibits a strong SOC-driven $J_{\rm eff} = 1/2$ Mott-insulating state, where the corner-sharing IrO_6 octahedra form a quasi-two-dimensional structure.[12] Na_2IrO_3, a candidate for the Kitaev spin model on the honeycomb lattice with edge-sharing IrO_6 octahedra, behaves as a geometrically frustrated magnet in proximity to a QSL state with strong spin entanglements.[7] For cubic $KSbO_3$-type $La_3Ir_3O_{11}$, the corner- and edge-sharing IrO_6 octahedra together construct a three-dimensional frustrated motif, in which each edge-sharing Ir_2O_{10} dimer has four connections to other dimers through corner-shared oxygens.[11] Early Mössbauer spectroscopy[13] and x-ray diffraction (XRD) experiments[11] on $La_3Ir_3O_{11}$ revealed that Ir ions formally take a nominal valence of 4.33+ as opposed to 4+. Recently, based on first-principles calculations, Singh and Pulikkotil predicted that $La_3Ir_3O_{11}$ hosts a SOC-driven semimetallic state composed of strongly hybridized Ir-5d and O-2p orbitals,[14] which was supported by electrical transport experiments carried out by Aoyama *et al.*[15] Nevertheless, more recently, Yang *et al.* proposed that $La_3Ir_3O_{11}$ could be a possible QSL candidate.[16]

The experimental verification of superconductivity evolving from QSL has become one of the central issues in condensed matter physics soon after Anderson proposed that the unconventional superconductivity in cuprates can evolve from the spin liquid state.[17] As one of the fundamental state parameters, pressure has been proved to be an effec-

*Project supported by the National Key Research and Development Program of China (Grant Nos. 2018YFA0305704 and 2016YFA0401804), the National Natural Science Foundation of China (Grant Nos. U1632275, U1932152, 11874362, 11704387, 11804344, 11804341, 11974016, U19A2093, and U1832209), the Natural Science Foundation of Anhui Province, China (Grant Nos. 1808085MA06, 2008085QA40, and 1908085QA18), the Users with Excellence Project of Hefei Center CAS (Grant No. 2020HSC-UE015), and the Collaborative Innovation Program of Hefei Science Center CAS (Grant No. 2020HSC-CIP014). A portion of this work was supported by the High Magnetic Field Laboratory of Anhui Province under Contract No. AHHM-FX-2020-02. Yonghui Zhou was supported by the Youth Innovation Promotion Association CAS (Grant No. 2020443).

†Corresponding author. E-mail: yhzhou@hmfl.ac.cn

‡Corresponding author. E-mail: zryang@issp.ac.cn

© 2021 Chinese Physical Society and IOP Publishing Ltd

tive and clean way to tune the crystal structure and the electronic states in iridates[18–23] and QSL candidates.[24–28] Very recently, a persistent insulating state at megabar pressures was reported in Sr_2IrO_4, which offers a perspective for understanding the discrepancies between theoretical proposals and experimental results in Sr_2IrO_4, including the absence of superconductivity.[18] More interestingly, recent high-pressure experimental investigations uncovered pressure-induced superconductivity in $NaYbSe_2$, which is a triangular QSL candidate.[27,28] For geometrically frustrated $La_3Ir_3O_{11}$, theoretical calculations predicted a semimetallic state[14] or a possible QSL state[16] at ambient pressure, while transport experiments showed a stable semimetallic behavior towards 13 GPa.[15] Because the maximum pressure applied in the resistivity measurements is 13 GPa and the high-pressure structure is not reported, the detailed correlation between the structure and electronic state as well as their evolutions under high pressure is still unclear.

In this work, we report the electronic and structural properties of $La_3Ir_3O_{11}$ by combining high-pressure electrical transport, synchrotron XRD, and Raman spectroscopy measurements. By extending the pressure up to 50–80 GPa, a semimetal–insulator transition is revealed at a critical pressure $P_c \sim 38.7$ GPa. It is shown that although the pristine $KSbO_3$-type structure is stable up to 73.1 GPa, the bulk modulus as well as the pressure dependence of bond length d_{Ir-Ir} displays changes around P_c. Consistently, Raman spectra show corresponding anomalies across P_c. Our results show that the local distortion of IrO_6 octahedra plays a key role in the emergent insulating behavior, by weakening electron hopping of pressurized $La_3Ir_3O_{11}$.

2. Experimental details

$La_3Ir_3O_{11}$ single crystals were grown by flux method.[15] The samples were first characterized at ambient pressure via electrical resistance, Raman spectrum, and energy dispersive x-ray spectroscopy (Fig. S1 in supplementary material). A standard four-probe method was employed to perform the high-pressure electrical transport measurements on single crystals of $La_3Ir_3O_{11}$ in a BeCu diamond anvil cell (DAC) with a rhenium gasket. The culet sizes of diamond were 300 μm. Sodium chloride (NaCl) powder was used as the pressure transmitting medium. High-pressure angle-dispersive synchrotron XRD and Raman scattering experiments were carried out in a Mao–Bell cell at room temperature. A pair of diamond in a diameter of 200 μm and rhenium gasket were used. Daphne 7373 served as the pressure transmitting medium. Synchrotron XRD experiments ($\lambda = 0.6199$ Å) were conducted at the beamline BL15U1, Shanghai Synchrotron Radiation Facility (SSRF). The final images were integrated via the DIOPTAS program[29] and standard Rietveld refinement method was used to fit the XRD patterns via the GSAS-II program.[30] Raman scattering measurements were performed at room temperature on a freshly cleaved single crystal using 532 nm solid-state laser for excitation with power below 10 mW to avoid any heating effect. The ruby fluorescence shift was used to calibrate the pressure at room temperature in all experiments.[31]

3. Results and discussion

Figures 1(a) and 1(b) show the selected temperature-dependent resistance $R(T)$ curves of $La_3Ir_3O_{11}$ single crystal at high pressures up to 53.8 GPa. At 0.3 GPa, the resistance first increases slightly with decreasing temperature, and then decreases remarkably followed by an upturn below 60 K. The nonmonotonic temperature dependence of resistance implies a semimetallic conductivity, which is in line with that case of ambient pressure in Fig. S1 as well as previous literature.[15] Here two characteristic temperatures T_p and T_d are marked by up and down arrows, respectively. With increasing pressure up to 18.1 GPa, the resistance over the whole temperature range decreases with both T_p and T_d being shifted to lower temperatures monotonically. This trend changes at 24.7 GPa, above which the resistance rises inversely, which can be seen clearly from the isothermal resistance curves at 5 K, 100 K, and 300 K in Fig. 1(c). When the pressure increases up to 38.7 GPa, the characteristic temperatures T_p and T_d almost disappear and the sample exhibits a complete insulating behavior. As the pressure is continuously increased from 38.7 GPa to 53.8 GPa, the insulating behavior maintains and the resistance globally gets enhanced, demonstrating a semimetal–insulator transition around 38.7 GPa.

To check the structural stability of pristine $La_3Ir_3O_{11}$ under pressure, we performed high-pressure synchrotron XRD measurements on crushed crystal powder. Figure 2(a) shows the representative diffraction patterns at room temperature. With increasing pressure up to 73.1 GPa, all the diffraction peaks move towards high angles and no peak splitting due to symmetry reduction can be detected throughout the whole pressure range studied. The XRD patterns can be refined by a standard Rietveld method with the cubic $KSbO_3$-type structure (space group *Pn*-3, No. 201). Figure 2(b) displays the schematic structure of $La_3Ir_3O_{11}$, in which each edge-sharing Ir_2O_{10} dimer has four connections to other dimers through corner-shared oxygens.[11] A representative refinement of the XRD patterns at 0.7 GPa is presented at the bottom of Fig. 2(a). Note that the exact position of oxygen atoms cannot be extracted in this XRD experiment due to low scattering power of oxygen atoms. Figure 2(c) shows the extracted volume and bond length d_{Ir-Ir} as a function of pressure. One can see that the pressure-dependent volume and

$d_{\mathrm{Ir-Ir}}$ consistently show a kink around 37.1 GPa. Meanwhile, the trend of bond angles does not display obvious change except some fluctuations (not shown here). This indicates that although the $KSbO_3$-type structure is stable under pressure, a subtle structural modification occurs in the pressurized $La_3Ir_3O_{11}$. The volume can be fitted well by the third-order Birch–Murnaghan equation of state,[32] which yields the ambient pressure volume $V_0 = 870.8$ (±0.8) Å^3, bulk modulus $B_0 = 229.6$ (±3.5) GPa for the low–pressure region of 0.7–37.1 GPa, and $V_0 = 840.3$ (±5.4) Å^3, $B_0 = 357.2$ (±23.0) GPa for the high-pressure region of 40.3–73.1 GPa. The first-order derivative of the bulk modulus at zero pressure, B_0', is fixed at 4 for all fittings. The structural modification is accompanied by an increment of bulk modulus $\Delta B_0/B_0 \sim 55.6\%$ at 37.1 GPa. Note that close to the critical pressure, the semimetal–insulator transition is observed (see Fig. 1).

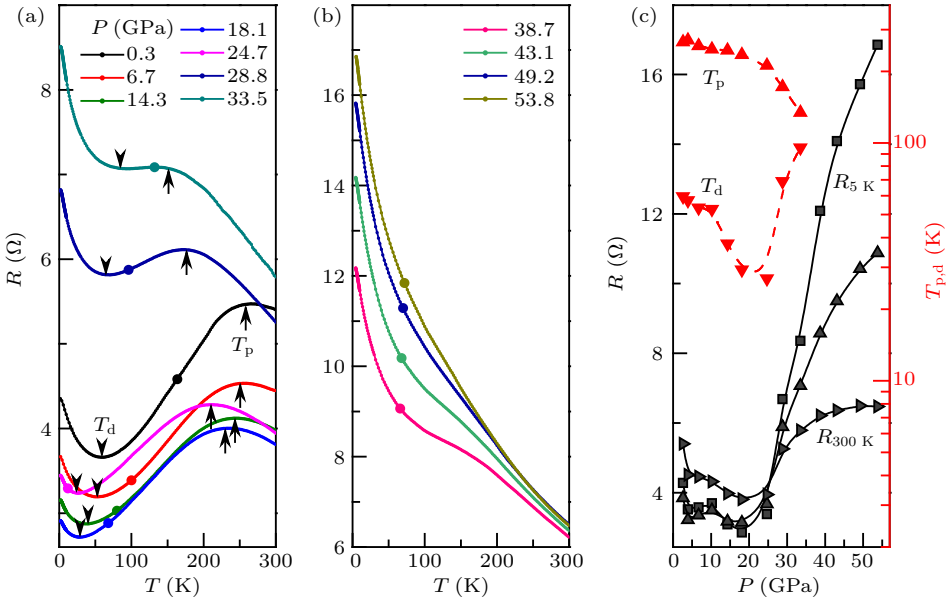


Fig. 1. Representative temperature-dependent electrical resistance $R(T)$ curves of $La_3Ir_3O_{11}$ at high pressures (a) below 33.5 GPa and (b) above 38.7 GPa, respectively. The characteristic temperatures T_p and T_d are marked by the vertical arrows, which are extracted the first derivative of resistance dR/dT. (c) Left: The isothermal resistance at 5 K, 100 K, and 300 K as a function of pressure. Right: The pressure dependence of temperatures T_p and T_d.

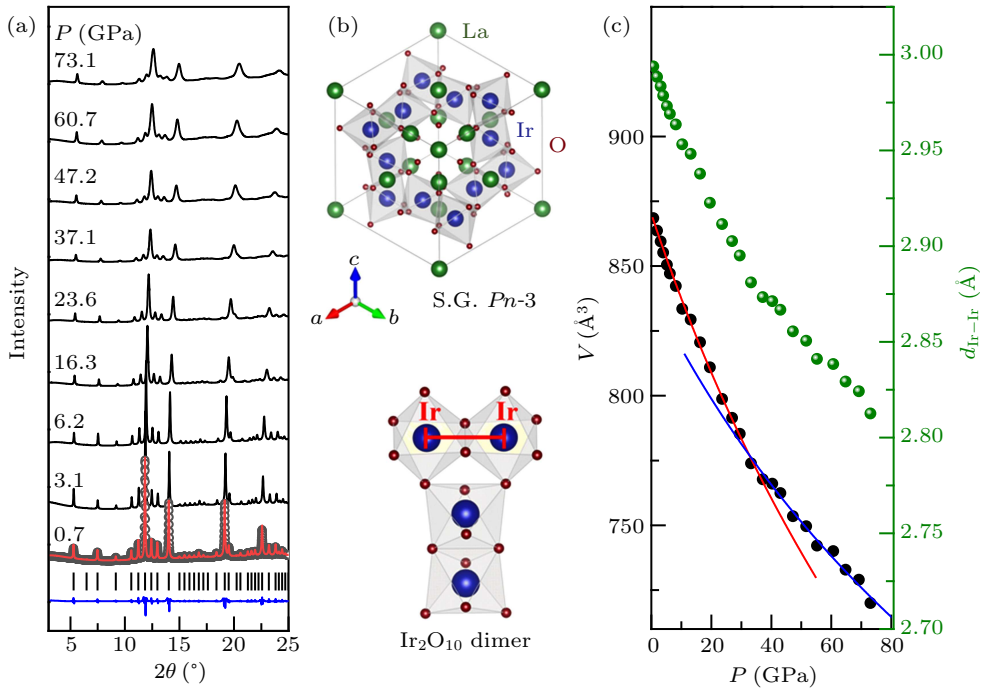


Fig. 2. (a) Room-temperature synchrotron XRD patterns ($\lambda = 0.6199$ Å) of $La_3Ir_3O_{11}$ under compression up to 73.1 GPa. For 0.7 GPa, the solid lines and open circles represent the Rietveld refinements for the lattice and observed data, respectively. The vertical bars symbolize the peak positions of cubic *Pn*-3 phase ($Z = 4$). (b) Upper: Schematic crystal structure of $La_3Ir_3O_{11}$ viewed along [111] direction. Lower: Enlarge view of Ir_2O_{10} dimer with two edge-sharing IrO_6. The Ir–Ir bond length $d_{\mathrm{Ir-Ir}}$ is denoted by the red line segment. (c) Pressure dependence of the volume and bond length $d_{\mathrm{Ir-Ir}}$. The red and blue solid lines represent the fitting results with the Birch–Murnaghan equation of states below and above 37.1 GPa, respectively. The orange and yellow regions are guides to the eyes.

Raman spectroscopy is an effective and powerful tool in detecting lattice vibrations, which can provide information including electron–phonon coupling, weak lattice distortion, and/or structural transition. We conducted room-temperature Raman scattering experiments for comparison with the XRD data. Figure 3(a) shows the selected Raman spectra of $La_3Ir_3O_{11}$ single crystal at high pressures. At 0.6 GPa, one can see that 13 Raman peaks appear in the frequency range of 170–1000 cm^{-1}, which is consistent with that case of ambient pressure. Here these peaks are named as M_{1-13}, considering no reference about the specific vibration modes in $La_3Ir_3O_{11}$. Consistent with XRD data, upon compression to 33.8 GPa, a discernable change in the relative intensity occurs between modes M_{10} and M_{12}, as denoted by the blue and red arrows, respectively. Namely, mode M_{12} becomes more and more weaker, while mode M_{10} becomes more and more stronger with increasing pressure across 33.8 GPa. In addition, mode M_2 exhibits a distinct redshift in the low-pressure region while turns back to blueshift above 33.8 GPa, which can be clearly discerned from the contour plot of Raman spectra in the frequency range of 170–300 cm^{-1} [see Fig. 3(b)].

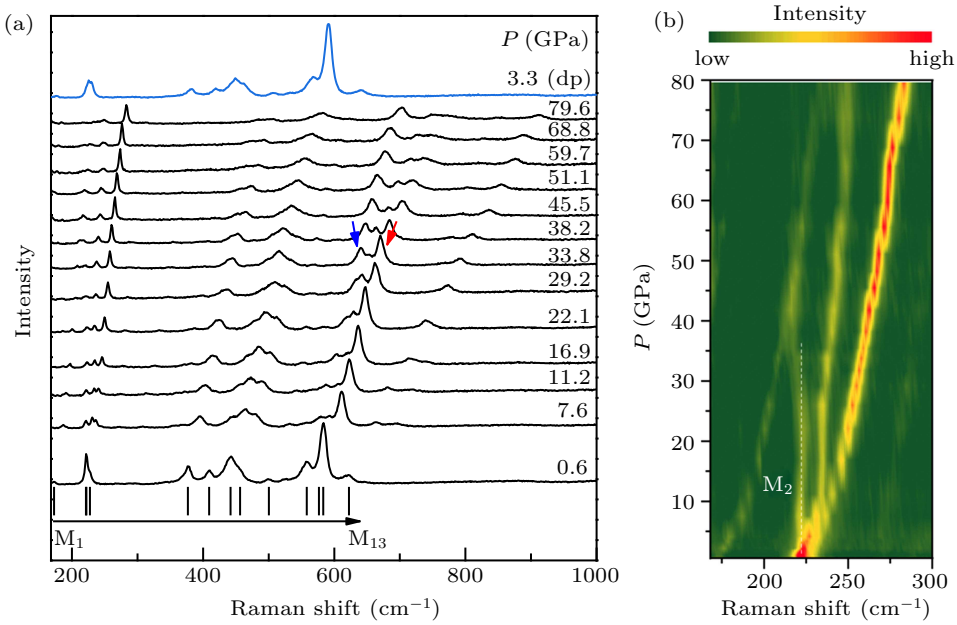


Fig. 3. (a) Selected room-temperature Raman spectra of $La_3Ir_3O_{11}$ single crystal under compression and decompression (denoted by "dp"). At 0.6 GPa, Raman modes named M_{1-13} are marked by the black vertical bars. At 33.8 GPa, the anomaly in intensity of Raman modes M_{10} and M_{12} is symbolized by the blue and red arrows, respectively. (b) Contour plot of Raman modes M_{1-4} under compression. For clarify, the frequency of Raman mode M_2 at 0.6 GPa is indicated by the vertical dashed line.

Figures 4(a) and 4(b) display the pressure-dependent frequency obtained from Lorentz fittings of the Raman peaks. Notably, all the modes except mode M_2 shift to higher frequencies monotonically. The pressure evolution of mode M_2 displays three different regions, i.e., two normal blueshift regions plus a redshift region (see the gray area). Concomitantly, the frequency of M_3 mode shows a kink in region II. We note that the abnormal evolutions of cubic $KSbO_3$-type $La_3Ir_3O_{11}$ deduced from our Raman spectra are very similar to the case of body-centered cubic $KSbO_3$, which were attributed to the distortion of SbO_6 octahedron at high pressures.[33] In the pressurized $La_3Ir_3O_{11}$, the occurrence of structural distortion is in accordance with the change of bulk modulus as well as anomaly in the pressure dependence of bond length d_{Ir-Ir}. Moreover, it can account for the abnormal insulating behavior. On one hand, it is commonly believed that the metallic state is favored at high pressures as the shrinkage of lattice normally enhances the band overlapping. On the other hand, the enhanced crystal distortion, i.e., rotation and tilting of IrO_6 octahedra, generally weakens electron hopping and can lead to localization. We note that the competition of these two forces renders Sr_2IrO_4 a persistent insulator at megabar pressures.[18]

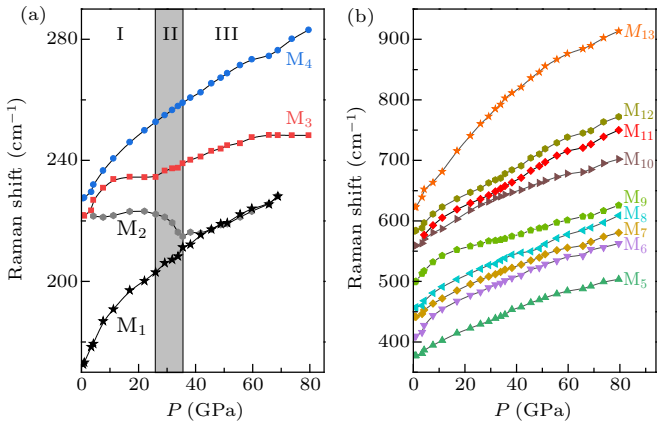


Fig. 4. The pressure dependence of low-frequency Raman modes M_{1-4} (a) and low-frequency Raman modes M_{5-13} (b). The pressure evolution of M_2 mode exhibits three distinct regions, i.e., two normal blueshift regions plus a redshift region.

4. Conclusion

In summary, we have investigated the pressure effect on the structural and electronic properties of geometrically frustrated iridate $La_3Ir_3O_{11}$ by combining high-pressure synchrotron XRD, Raman scattering, and electrical transport experiments, from which a critical pressure $P_c \sim 38.7$ GPa was revealed. We observed a semimetal–insulator transition at P_c, which can be further correlated to the appearance of structural distortion. Our work emphasizes a unique, ultra-important role that the lattice plays in determining the ground state in spin–orbit-coupled materials.

Acknowledgments

A portion of this work was supported by the High Magnetic Field Laboratory of Anhui Province. We thank Zhaoming Tian for affording the single crystals. We thank Lili Zhang for supporting our XRD experiments. The high-pressure synchrotron x-ray diffraction experiments were performed at beamline BL15U1, Shanghai Synchrotron Radiation Facility.

References

[1] Cao G and Schlottmann P 2018 *Rep. Prog. Phys.* **81** 042502
[2] Pesin D and Balents L 2010 *Nat. Phys.* **6** 376
[3] Wan X, Turner A M, Vishwanath A and Savrasov S Y 2011 *Phys. Rev. B* **83** 205101
[4] Kim B J, Ohsumi H, Komesu T, Sakai S, Morita T, Takagi H and Arima T 2009 *Science* **323** 1329
[5] Okamoto Y, Nohara M, Aruga-Katori H and Takagi H 2007 *Phys. Rev. Lett.* **99** 137207
[6] Chaloupka J, Jackeli G and Khaliullin G 2010 *Phys. Rev. Lett.* **105** 027204
[7] Choi S K, Coldea R, Kolmogorov A N, Lancaster T, Mazin I I, Blundell S J, Radaelli P G, Singh Y, Gegenwart P, Choi K R, Cheong S W, Baker P J, Stock C and Taylor J 2012 *Phys. Rev. Lett.* **108** 127204
[8] Rau J G, Lee E K-H and Kee H-Y 2016 *Annu. Rev. Condens. Matter Phys.* **7** 195
[9] Moon S J, Jin H, Kim K W, Choi W S, Lee Y S, Yu J, Cao G, Sumi A, Funakubo H, Bernhard C and Noh T W 2008 *Phys. Rev. Lett.* **101** 226402
[10] Ramirez A P 1994 *Annu. Rev. Mat. Sci.* **24** 453
[11] Abraham F, Trehoux J and Thomas D 1979 *J. Less-Common Metals* **63** 57
[12] Kim B J, Jin H, Moon S J, Kim J Y, Park B G, Leem C S, Yu J, Noh T W, Kim C, Oh S J, Park J H, Durairaj V, Cao G and Rotenberg E 2008 *Phys. Rev. Lett.* **101** 076402
[13] Abraham F, Trehoux J, Thomas D and Wagner F E 1982 *J. Less-Common Metals* **84** 245
[14] Singh V and Pulikkotil J J 2017 *Mater. Chem. Phys.* **186** 592
[15] Aoyama T, Emi K, Tabata C, Nambu Y, Nakao H, Yamauchi T and Ohgushi K 2019 *J. Phys. Soc. Jpn.* **88** 093706
[16] Yang J, Wang J R, Zhen W L, Ma L, Ling L S, Tong W, Zhang C J, Pi L and Zhu W K 2019 *Phys. Rev. B* **100** 205107
[17] Anderson P W 1987 *Science* **235** 1196
[18] Chen C, Zhou Y, Chen X, Han T, An C, Zhou Y, Yuan Y, Zhang B, Wang S, Zhang R, Zhang L, Zhang C, Yang Z, DeLong L E and Cao G 2020 *Phys. Rev. B* **101** 144102
[19] Haskel D, Fabbris G, Zhernenkov M, Kong P P, Jin C Q, Cao G and van Veenendaal M 2012 *Phys. Rev. Lett.* **109** 027204
[20] Ding Y, Yang L, Chen C C, Kim H S, Han M J, Luo W, Feng Z, Upton M, Casa D, Kim J, Gog T, Zeng Z, Cao G, Mao H K and van Veenendaal M 2016 *Phys. Rev. Lett.* **116** 216402
[21] Hermann V, Ebad-Allah J, Freund F, Pietsch I M, Jesche A, Tsirlin A A, Deisenhofer J, Hanfland M, Gegenwart P and Kuntscher C A 2017 *Phys. Rev. B* **96** 195137
[22] Hermann V, Altmeyer M, Ebad-Allah J, Freund F, Jesche A, Tsirlin A A, Hanfland M, Gegenwart P, Mazin I I, Khomskii D I, Valentí R and Kuntscher C A 2018 *Phys. Rev. B* **97** 020104
[23] Hermann V, Ebad-Allah J, Freund F, Jesche A, Tsirlin A A, Gegenwart P and Kuntscher C A 2019 *Phys. Rev. B* **99** 235116
[24] Kurosaki Y, Shimizu Y, Miyagawa K, Kanoda K and Saito G 2005 *Phys. Rev. Lett.* **95** 177001
[25] Shimizu Y, Hiramatsu T, Maesato M, Otsuka A, Yamochi H, Ono A, Itoh M, Yoshida M, Takigawa M, Yoshida Y and Saito G 2016 *Phys. Rev. Lett.* **117** 107203
[26] Hu K, Zhou Z, Wei Y W, Li C K and Feng J 2018 *Phys. Rev. B* **98** 100103
[27] Zhang Z, Yin Y, Ma X, Liu W, Li J, Jin F, Ji J, Wang Y, Wang X, Yu X and Zhang Q 2020 arXiv:2003.11479
[28] Jia Y T, Gong C S, Liu Y X, Zhao J-F, Dong C, Dai G Y, Li X D, Lei H C, Yu R Z, Zhang G M and Jin C Q 2020 *Chin. Phys. Lett.* **37** 097404
[29] Prescher C and Prakapenka V B 2015 *High Pressure Res.* **35** 223
[30] Toby B H and Von Dreele R B 2013 *J. Appl. Cryst.* **46** 544
[31] Mao H K, Xu J and Bell P M 1986 *J. Geophys. Res.* **91** 4673
[32] Birch F 1947 *Phys. Rev.* **71** 809
[33] Zhao H, Tan D, Tian Y, He Y, Li Y, Li X, Yang K, Chen B and Xiao W 2018 *High Pressure Res.* **38** 232